Proceedings of 16th International Symposium on Unsteady Aerodynamics, Aeroacoustics & Aeroelasticity of Turbomachines
ISUAAAT16
19-23 September 2022, Toledo, Spain

ISUAAAT16-044

COUPLED SIMULATION OF A SHROUDED TURBINE BLADE ROW WITH CONTACT FRICTION INTERFACES - ANALYSIS OF A LIMIT TORUS OSCILLATION

Christian Berthold*
Institute of Propulsion Technology
German Aerospace Center (DLR)
Cologne, Germany

Christian Frey
Institute of Propulsion Technology
German Aerospace Center (DLR)
Cologne, Germany

ABSTRACT

In order to increase efficiency and achieve lighter engines, turbine blades are currently developed with a higher aerodynamic loading and tip Mach number which further increases flutter probability. Thus, modern and innovative turbine concepts include flutter-tolerant designs which limit the flutter induced vibration amplitudes to an acceptable level due to intentional friction in contact interfaces, which can lead to limit state vibrations, where the dissipation due to friction balances the aerodynamic excitation. Among several the possible limit states, this work focuses on the analysis of a Limit Torus Oscillation (LTO). Therefore, a fully coupled simulation of a turbine blade row with nonlinear contact interactions in the shroud is studied. An initial blade vibration evolves to an LTO. The harmonic content of the converged LTO is studied and a certain pattern of the participating harmonics is observed. Moreover the aerodynamic forces are investigated with respect to the interaction among the fluid waves of the quasi-periodic motion.

INTRODUCTION

In turbomachinery, blade vibrations are a major issue and must be considered during the design phase of new mechanical components. The three major mechanisms are flutter, forced response and non-synchronous vibrations. The focus of this work lies on flutter, which denotes self-excited vibrations of blades due to the interaction between the surrounding fluid and the blade's motion. Especially blades with a high aspect ratio as found in fans or low pressure turbines are prone to flutter.

In the past, the energy method was used in order to evaluate mechanical designs of turbomachinery components with the goal to avoid flutter at all costs. This however leads to a very narrow design space of the blades.

In order to increase efficiency and achieve lighter engines, turbine blades are currently developed with a higher aerodynamic loading and tip Mach number which further increases flutter probability [1, 2]. Thus, modern and innovative turbine concepts include flutter-tolerant designs which limit the flutter induced vibration amplitudes to an acceptable level due to intentional friction in contact interfaces in the blade root joints, underplatform dampers or shroud contact interfaces [3]. Thus limit state vibrations (e.g. a limit cycle oscillation) will arise [4,5], where the dissipation due to friction balances the aerodynamic excitation. The prediction of limit states and the resulting vibration amplitudes are of interest for engineers in order to evaluated a design with respect to high cycle fatigue. Due to the highly nonlinear behavior of the structure however, conventional methods like the energy method, the influence coefficient method or similar methods cannot be applied. These methods do not model the impact of nonlinear contact forces/dissipation on the mode shape and vibration frequency, which is important especially for shrouded turbines with contact interfaces. The mode shape and frequency, in turn, strongly influence the aerodynamic forces acting on the blade itself. As a result, the struc-

*Address all correspondence to this author.

tural motion and the fluid interact with each other, which must be accounted for, when strong nonlinear effects are expected.

Time Domain Fluid-Structure Interaction (TD-FSI) simulation methods are in principle able to resolve all these nonlinear effects and allow the coupled system to converge to any stable limit state, however they come at high computational costs [6]. In [7, 8] LCOs and stability limits (unstable LCOs from energy balance considerations) are investigated with a refined nonlinear modal analysis method based on [9] and a bidirectionally coupled Frequency Domain Fluid-Structure Interaction (FD-FSI) solver was developed, which is able to capture the nonlinear interactions between the fluid and the structure. An LCO only has a single fundamental frequency ω, and the motion can be expressed as a Fourier series:

$$\boldsymbol{u}(t) = \Re\left\{\sum_{k=-\infty}^{+\infty} \hat{\boldsymbol{u}}_k e^{\mathrm{i}k\omega t}\right\} \tag{1}$$

The investigation of the stability of limit states (see e.g. [10, 11]) however shows that an LCO which appears to be stable from energy balance considerations (as determined by the FD-FSI solver) can nevertheless be asymptotically unstable. An asymptotically unstable LCO does not necessarily mean that unbounded growth of the vibration amplitude occurs. It can also collapse into another stable LCO, Limit Torus Oscillations (LTO) or chaotic motion. Thus the coupled analysis of LTOs, where two or more incommensurable fundamental frequencies present in the limit state, is also an important topic for the evaluation of turbine blade row designs. In the case of two fundamental frequencies, ω_1 and ω_2, the quasi-periodic motion of an LTO can be represented as

$$\boldsymbol{u}(t) = \Re\left\{\sum_{(j,k)\in\mathscr{H}} \hat{\boldsymbol{u}}_{j,k} e^{\mathrm{i}(j\omega_1 + k\omega_2)t}\right\}, \quad \mathscr{H} = \mathbb{Z}^2. \tag{2}$$

So far, flutter induced LTOs were studied in [12, 13] with a simplified blade row model (with a single mode shape per wave number and linearized aerodynamic influence or even simpler). As mentioned above however, the nonlinear fluid-structure interactions can potentially lead to qualitative and quantitative different results compared to reduced models or uni-directional coupled methods. Since the previously developed FD-FSI solver is based on the classical harmonic balance method, it is limited to a single fundamental frequency, which makes it unsuitable for the simulation of LTOs, where two or more incommensurable base frequencies exist. Instead, for fully coupled FSI simulations, one must resort to computationally costly TD-FSI solvers.

In this work a fully coupled FSI simulation of a flutter induced LTO of a shrouded turbine blade row is studied in order to gain some insight into the coupling between the fluid and the structure. Past research showed that LTOs occur due to nonlinear structural forces in shroud contact interfaces or at the blade root, which leads to a coupling of waves with different nodal diameter and incommensurable frequencies. In these studies however, the aerodynamic forces have only been modeled with linear aerodynamic influence coefficients. An open question is the validity of this assumption for LTOs of turbine blades. Therefore the harmonic content of the converged LTO will be studied and also the aerodynamic forces are investigated with respect to the interaction among the different harmonics on the fluid side.

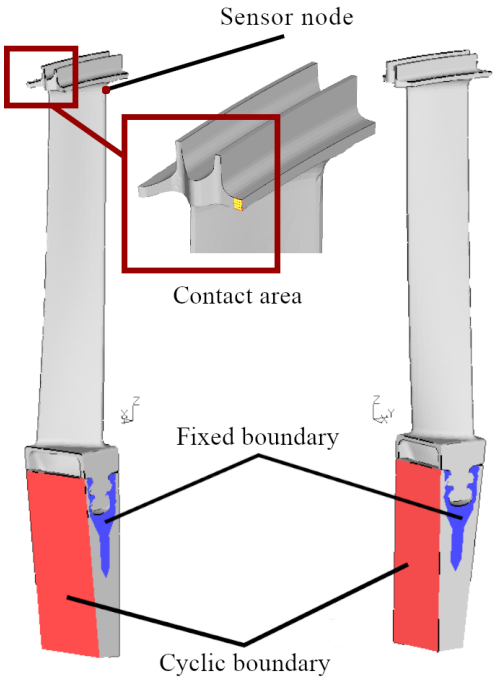

FIGURE 1: Structural model with a detailed view of the contact area (yellow) in the shroud [7]

METHODOLOGIES AND NUMERICAL MODEL

Structure Model

The investigated low pressure turbine (LPT) blade row (provided by MTU Aero Engines) has 60 tuned blades with interlocked tip shrouds. The structure is described using a Finite Element (FE) model with 33634 FE nodes and 25194 second order tetrahedral elements per sector. In the shroud a contact interface is located between each two neighbouring blades. One sector is illustrated in Fig. 1.

In a preprocessing step a static equilibrium under centrifu-

gal loading due to the rotation speed is computed. This static equilibrium serves as a reference configuration for the following dynamic force balance:

$$\boldsymbol{M}_{\mathrm{FE}}\ddot{\boldsymbol{q}}_{\mathrm{FE}} + \boldsymbol{K}_{\mathrm{FE}}\boldsymbol{q}_{\mathrm{FE}} + \boldsymbol{f}^{\mathrm{c}}_{\mathrm{FE}} = \boldsymbol{f}^{\mathrm{a}}_{\mathrm{FE}}. \tag{3}$$

The elastic forces are linearized which implies a linear material behavior and linear kinematics and thus the model is only suitable for small vibrations. The sparse, symmetric and positive definite matrices $\boldsymbol{M}_{\mathrm{FE}}$ and $\boldsymbol{K}_{\mathrm{FE}}$ are the mass and the stiffness matrix respectively and $\boldsymbol{q}_{\mathrm{FE}}$ denotes the FE nodal displacement coordinates (which are zero for the static equilibrium). $\boldsymbol{f}^{\mathrm{c}}_{\mathrm{FE}}$ and $\boldsymbol{f}^{\mathrm{a}}_{\mathrm{FE}}$ are the contact and aerodynamic forces. Furthermore Coriolis forces are neglected on the structural side. In the illustration of the sector model the region where fixed boundary conditions are applid is coloured in blue. Close to this region the fir-tree root is located. In the current model the blade is attached to the disk via fixed contact constraints.

In the contact area (marked yellow in Fig. 1) the normal relative displacement is constrained. Here spatial dry friction is modeled using coupled 2-dimensional elastic Coulomb elements with a constant normal load, also known as Jenkins elements [14, 15], which have a hysteretic force-displacement relationship. Thus, one obtains two relative degrees of freedom per contact element, which describe the relative motion in the tangential plane. Each of the 25 contact elements is connecting two neighboring nodes in the contact interface (both neighboring contact patches contain 25 FE nodes). For the contact model, the stiffness parameter is chosen very large. The eigenfrequencies of the FE model with tied contact and of the FE model with the contact stiffness of the contact elements deviate by approximately 0.001 %. The tangential force at which the transition from stick to slip occurs is denoted as F_{friction} and is also used for nondimensionalization. In Fig. 1 also a sensor node is indicated at which the blade displacement is evaluated for subsequent analysis and illustration. Furthermore the blade length L_B and the frequency of the lowest eigenmode f_{ref} are used for non-dimensionalization.

To reduce the number of unknowns in Eq. (3) a modal reduction according to $\boldsymbol{q}_{\mathrm{FE}} = \boldsymbol{\Psi}\boldsymbol{q}$ is used with $\boldsymbol{\Psi}$ containing all selected modeshapes and $\boldsymbol{q}$ denoting the modal coordinates. Substituting this transformation into Eq. (1) and subsequent Galerkin projection (modal truncation) yields a Reduced Order Model (ROM):

$$\boldsymbol{M}\ddot{\boldsymbol{q}} + \boldsymbol{K}\boldsymbol{q} + \boldsymbol{f}^{\mathrm{c}} = \boldsymbol{f}^{\mathrm{a}}. \tag{4}$$

The ROM is truncated such that the first 10 mode families are retained for each fundamental nodal diameter. During the eigenvalue analysis for the construction of $\boldsymbol{\Psi}$, the nonlinear

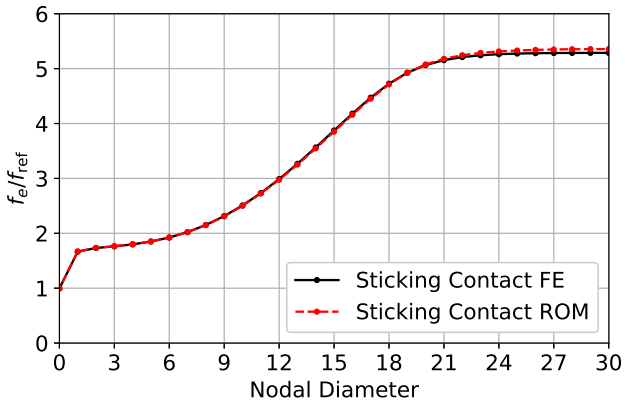

FIGURE 2: Lowest eigenfrequency of the linearized structure (FE model and ROM) for each ND. [16]

contact forces $\boldsymbol{f}^{\mathrm{c}}_{FE}$ and the aerodynamic forces $\boldsymbol{f}^{\mathrm{a}}_{FE}$ are neglected (frictionless sliding of the contact surfaces is allowed). In order to calculate the modal contact forces of the ROM $\boldsymbol{f}^{\mathrm{c}}$, the contact forces in FE space are projected onto the modal basis: $\boldsymbol{f}^{\mathrm{c}} = \boldsymbol{\Psi}^{\mathrm{T}}\boldsymbol{f}^{\mathrm{c}}_{FE}$. The modal displacements and velocities $\boldsymbol{q}$ and $\dot{\boldsymbol{q}}$ are combined in $\boldsymbol{u}^{\mathrm{s}} = [\boldsymbol{q}; \dot{\boldsymbol{q}}]$.

In a preprocessing step an interpolation matrix $\boldsymbol{T}$ is constructed using bilinear basis functions which maps the mode shape displacements $\boldsymbol{\Psi}$ from the structural mesh at the fluid-structure interface Γ onto the fluid mesh vertices. During the coupled simulation the modal aerodynamic force vector is then simply evaluated according to $\boldsymbol{f}^{\mathrm{a}} = (\boldsymbol{T}\boldsymbol{\Psi}|_{\Gamma})^{\mathrm{T}}\boldsymbol{f}^{\mathrm{a}}_{\mathrm{FVM}}$ with $\boldsymbol{f}^{\mathrm{a}}_{\mathrm{FVM}}(\boldsymbol{u}^{\mathrm{a}})$ containing the vertex based forces due to the surface pressure of the fluid mesh (the traction forces are neglected since they are small compared to the pressure).

For small vibrations the contact elements remain in sticking conditions and the structure behaves linearly. Then only the stiffness parameter of the contact elements is relevant. Since the truncation to a moderate number of normal modes leads to an underprediction of the static compliance to loads applied at the contact interface, the eigenfrequencies of the modes with sticking contacts are much higher than of the unreduced FE model. Thus, for the ROM, the stiffness parameter of the Jenkins elements is reduced such that the lowest linear eigenfrequency f_e for each Nodal Diameter (ND) is similar to the one from the FE model, cf. Fig. 2. Notice that $f_{\mathrm{ref}} = f_e(\mathrm{ND} = 0)$ from the ROM and is used for nondimensionalization throughout this work. It is emphasized that a substructuring technique like the Craig-Bampton method [17] performs more accurately in the nonlinear regime (at greater amplitudes) than a modally truncated ROM. For the present study including numerical time integration however a modal ROM is more suitable because of the relatively high numerical stiffness due to the artificial high-

frequency components associated with the component modes of the Craig-Bampton method.

Aerodynamic Model

The fluid is modeled with the compressible unsteady Reynolds-averaged Navier-Stokes (URANS) equations

$$\frac{d\boldsymbol{u}^{\mathrm{a}}}{dt} + \boldsymbol{R}(\boldsymbol{u}^{\mathrm{a}}, \boldsymbol{u}^{\mathrm{s}}) = 0 \tag{5}$$

where $\boldsymbol{u}^{\mathrm{a}}$ is the vector of conservative variables and $\boldsymbol{R}$ contains the spatial discretization of the URANS equations. Ideal gas is assumed and a $k-\omega$ turbulence model [18] is used. For the spatial discretization of the fluid domain 862,848 finite volume cells for a single sector and 51×10^6 cells for the full blade row are used. For the boundary treatment at the inlet and exit of the fluid domain, 1-dimensional fluid NRBCs [19] are chosen to avoid the above mentioned disadvantages (they do not require a fundamental frequency). Furthermore their implementation is consistent in the frequency and time domain modules of the fluid solver which is important in order to compare frequency and time domain simulations.

The fluid mesh deformation at the fluid-structure interface $\boldsymbol{U}|_\Gamma$ (the blade surface) is computed from the modal displacements according to $\boldsymbol{U}|_\Gamma = \boldsymbol{T}\boldsymbol{\Psi}|_\Gamma \boldsymbol{q}$ (and analogously the surface velocity $\dot{\boldsymbol{U}}|_\Gamma = \boldsymbol{T}\boldsymbol{\Psi}|_\Gamma \dot{\boldsymbol{q}}$). The interior of the fluid mesh must be deformed appropriately upon each coupling iteration in order to follow the blades' surface. This is achieved by solving a Laplace equation with the deformed blade surface $\boldsymbol{U}|_\Gamma$ as boundary condition on the fluid mesh. The arbitrary Langrangian-Eulerian form of the finite volume formulation is used to take the mesh motion into account.

In Fig. 3 the Mach number contour at a channel height of 85% is shown. The total pressure ratio amounts to 1.16 (in the absolute frame of reference). By prescribing a relatively low static pressure at the exit a transonic point of operation with a shock on the suction side is achieved, which leads to an increased fluid velocity and thus to a low reduced frequency [20]. A low exit pressure also favours a high blade loading which further increases flutter intensity. The low reduced frequency and high aerodynamic blade loading leads to a strong aerodynamic excitation of the blade row.

The fluttercurve is presented in Fig. 4 which shows the aerodynamic damping ratio

$$D_{\mathrm{a}} = \frac{W_{\mathrm{a}}}{4\pi E_{\mathrm{kin,max}}} \tag{6}$$

as function of the ND for the linearized structure ROM (with sticking contact conditions in the shroud) with W_{a} denoting the aerodynamic work per cycle and $E_{\mathrm{kin,max}}$ being the maximum kinetic energy of the mode. It can be observed that blade vibrations are aerodynamically unstable for travelling wave modes with ND between 3 and 19.

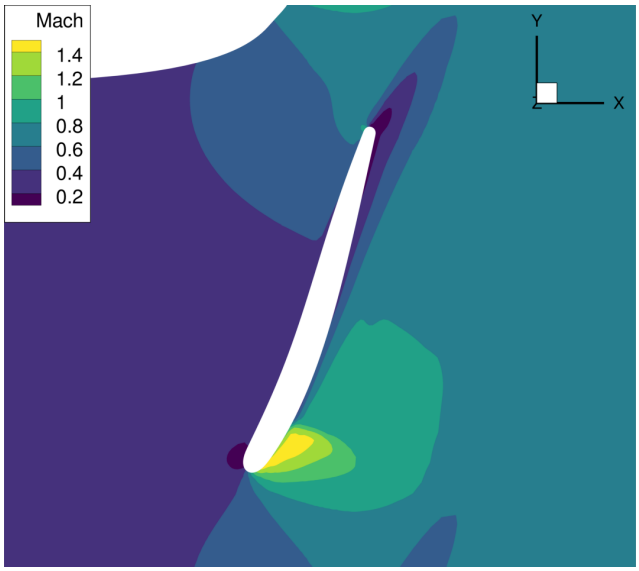

FIGURE 3: Mach number contour at 85% channel height. [16]

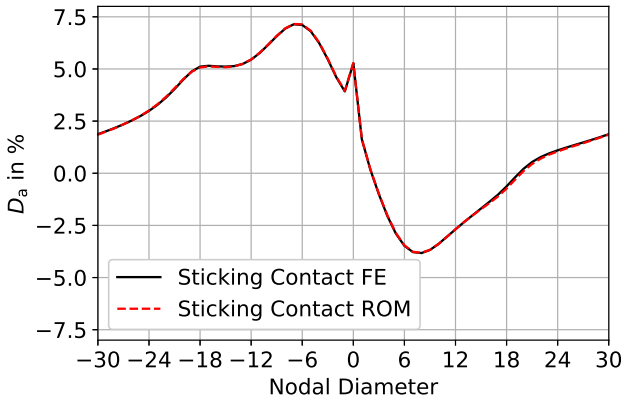

FIGURE 4: Fluttercurve of the linearized structure (FE model and ROM) for the first mode. [16]

Analogous to the comparison of the eigenfrequencies of the linearized structure in Fig. 2 also the aerodynamic damping ratio D_{a} is evaluated for the FE model and the ROM and plotted in Fig. 4. The good agreement shows that the aerodynamic behavior is suprisingly good described also with the structural ROM.

Due to the nonlinear flow features, D_{a} is not constant (as it would be in the case of perfectly linear aerodynamic forces) but

depends on the modal amplitude . This dependency is investigated and found to be only small compared to the structural damping. D_a varies not more than 8 % relative to a reference value picked for a very small amplitude.

TD-FSI Solver

The TD-FSI solver consists out of the flow solver TRACE and a custom structural solver written in python. The two solvers are coupled by a sequential fixed-point algorithm [21] and is illustrated in Fig. 5. For each physical timestep a fixed amount of coupling iterations is performed which ensures sufficient convergence. A single coupling iteration consists of 4 steps (denoted 1 to 4 in Fig. 5).

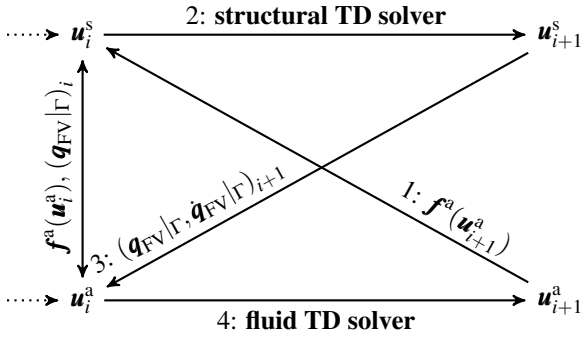

FIGURE 5: TD-FSI coupling scheme [16]

At the beginning (step 1) the modal aerodynamic force $\boldsymbol{f}^\mathrm{a}(\boldsymbol{u}_{i+1}^\mathrm{a})$ at the next time step t_{i+1} is calculated and passed to the structural solver. In case of a physical time step's primary coupling iteration, $\boldsymbol{f}^\mathrm{a}(\boldsymbol{u}_{i+1}^\mathrm{a})$ is linearly extrapolated from the last two time steps. In step 2 the structural solver calculates the modal state variables $\boldsymbol{u}_{i+1}^\mathrm{s}$ for the next time step by integrating Eq. (4) w.r.t. time. Subsequently (step 3) the fluid-structure interface $\boldsymbol{U}|_\Gamma$ (the blade surface) and the fluid mesh are deformed according to the updated structural state variables. In step 4 the flow solver then calculates the conservative fluid variables $\boldsymbol{u}_{i+1}^\mathrm{a}$ for the next time step . Finally the next coupling iteration starts with step 1 or, after three coupling iterations, the next physical time step is advanced ($i \leftarrow i+1$). Three coupling iterations turned out to be sufficient for the studied testcase because for further iterations the residual of the fluid solver does not rise above a very low level anymore (even directly after new displacements have been received).

The tuned bladerow's motion can be described with traveling wave coordinates [14]. In the time domain a traveling wave can be viewed as the superposition of two linearly independent standing waves (except ND 0 and 30 which are standing waves themselve in case of an even amount of 60 blades). Thus there are 29 traveling waves (traveling forward or backward) and two standing waves for ND 0 and 30 for each mode family. When the structural motion is approximated with 10 mode families, a corresponding real system as required for time domain treatment must have $(29 \cdot 2 + 1 + 1) \cdot 10 = 600$ modes. Thus, the ROM for the full blade row described in Eq. (4) has 600 DOFs.

The time derivatives of Eq. (4) are discretized using the Newmark scheme [22] with average constant acceleration. The resulting nonlinear system of equations is solved with a predictor-corrector like method. In the predictor step the nonlinear contact forces $\boldsymbol{f}^\mathrm{c}$ are linearized with the stiffness of the contact model and the state variables are calculated for the next time step. In the subsequent corrector step the contact forces are re-evaluated according to their differential formulation and the next time step is calculated for a second time. Thus the resolution of the stick-slip transitions is limited by the time step length used for numerical integration. For reasonable accuracy each time step of the TD-FSI solver is always subdivided into 8 increments for the structural solver. For the increments, $\boldsymbol{f}^\mathrm{a}$ is linearly interpolated between $\boldsymbol{f}_i^\mathrm{a}$ and $\boldsymbol{f}_{i+1}^\mathrm{a}$.

The flow solver uses a pseudo-time stepping method in order to solve the nonlinear system of equations arising from the finite volume discretization of the Navier-Stokes equations. The temporal terms are discretized with the second order backward differentiation formula (BDF2).

In the current study the modal aerodynamic forces connected to modes with ND 0 (which contain the steady part) are not passed to the structural solver. The same simplification is done for the other direction: the deflection of modes with ND 0 (due to structural nonlinearities) is not represented in the aerodynamic model. These simplifications reduce the complexity of the coupled system. A coupling of modes with ND 0 between the two solvers would induce a change in the point of operation of the engine. This level of complexity is not yet intended and spared for future research. Additionally this would significantly increase the time needed to achieve a periodic steady state. All DOFs connected to ND 0 are still part of the solution within each physical domain.

Frequency Domain Methods

Currently there is no method available for a bidirectionally-coupled frequency domain FSI simulation of nonlinear turbine blade vibrations with two or more incommensurable frequencies. In the current study however, isolated waves of the LTO are investigated and compared to the time domain LTO result, in order to obtain a first estimate of the degree of coupling among the different fundamental fluid waves. For the computations of the isolated waves the Harmonic Balance (HB) method is used, which approximates

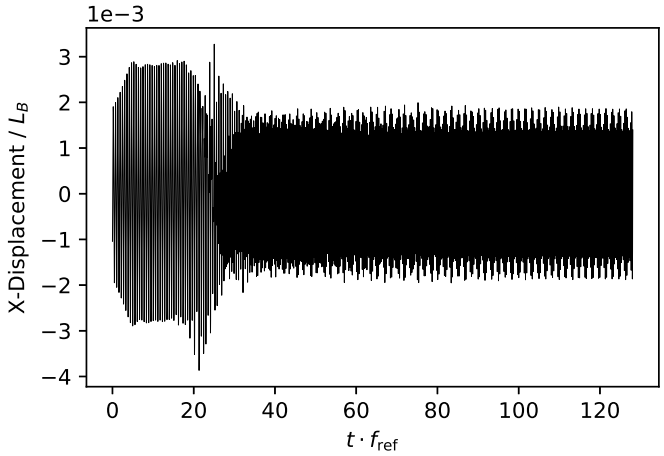

FIGURE 6: X-Displacement over time at sensor node for LTO12-14-16. [16]

the solution by a truncated Fourier series:

$$\boldsymbol{u}^{\mathrm{a}}(t) \approx \Re\left\{\sum_{k=0}^{H^{\mathrm{a}}} e^{ik\omega t}\hat{\boldsymbol{u}}_k^{\mathrm{a}}\right\}. \tag{7}$$

$\hat{\boldsymbol{u}}_k^{\mathrm{a}}$ denotes the k-th harmonic complex Fourier coefficient vector of the state variables and H^{a} the number of harmonics used for the approximation. The semi-discrete Navier-Stokes equations are transformed into the frequency domain by means of the Harmonic Balance (HB) method [23]. The alternating frequency-time (AFT) scheme is used to deal with all nonlinear terms. Due to the assumed traveling wave motion of the fluid and the structure, only a single sector of the blade row must be modeled which drastically reduces the computational effort. For consistency, the structural modes of ND 0 are not represented in a HB fluid simulation.

MAIN RESULTS

The initial intent was to investigate an LCO of ND 3 by using an appropriate traveling wave motion as initial condition. The evolution of the X-displacement over time depicted in Fig. 6 shows two transitions. The first one occurs at the very beginning when the exponential growth stops and the vibrations start settling for an LCO with ND 3. In a second transition (starting at $t \cdot f_{\mathrm{ref}} \approx 20$) the vibration disintegrates and an LTO starts to develop. A 2D Fourier transform analysis of the quasi-periodic motion is shown in Fig. 7. The spectrum of Z-displacement at the sensor node reveals a "basic wave package" containing several fundamental waves centered around NDs 12, 14 and 16. A linear combination with the same coefficients

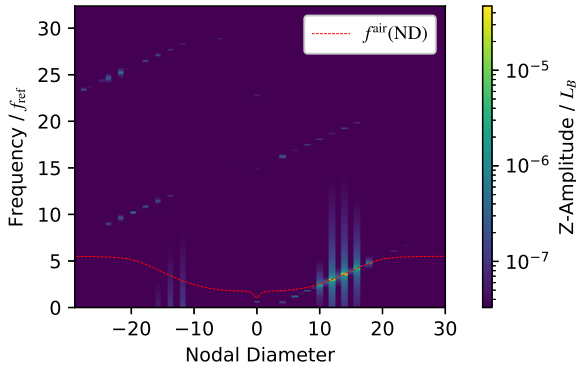

FIGURE 7: 2D-DFT of Z-Displacement at sensor node for LTO12-14-16. [16]

for frequencies and NDs among the waves of the "basic wave package" can be observed as in [13] and the same also holds for smaller peaks in this package (next to the three dominating ones). Furthermore, the spectrum also exhibits small contributions of higher harmonics, which are grouped in three distinct wave packages above the basic wave package. Investigation of the spectrum shows, that the LTO has two fundamental frequencies as in Eq. (2). ω_1 and ω_2 can be chosen arbitrarily and all participating wave frequencies can be obtained by a linear combination of the two weighted with signed integer coefficient. These coefficients correspond to elements in the space of the harmonic coefficients $\mathscr{H}$, cf. Eq. (2), but in the current case only a finite amount of harmonics participate significantly and thus $\mathscr{H}$ is only a small subset of $\mathbb{Z}^2$. Given the Fourier basis in Eq. (2), the harmonic indices are distributed in $\mathbb{Z}^2$ over a relatively wide range. Interestingly, when the Fourier space for a motion with two fundamental frequencies is expressed by an appropriate Fourier basis

$$\boldsymbol{u}^{\mathrm{s}}(t) \approx \sum_{(l,m)\in\mathscr{K}} \hat{\boldsymbol{u}}_{l,m}^{\mathrm{s}} e^{i(m\omega_0 + l\Delta\omega)t}, \quad \mathscr{K} \subset \mathbb{Z}^2, \tag{8}$$

with $\Delta\omega/(2\pi) = \Delta f = 0.3 f_{\mathrm{ref}}$ and $\omega_0/(2\pi) = f_{\mathrm{ND14}}$, the relevant harmonic indices space can be identified as $\mathscr{K} = (-6,-4,-2,0,2,4) \times (1,3,5,7)$, which suddenly is a very compact grid in $\mathbb{Z}^2$ compared to the conventional Fourier basis (cf. Eq. (2)). The index l describes harmonics within a single wave package while the index m refers to on of the four wave packages shown in Fig. 7. Obviously, the frequencies of the dominant participating harmonics are close to the eigenfrequencies of the modes (red line in Fig. 7) but it is interesting to see that the frequencies (and analogously NDs) of all participating harmonics follow the above relation even when there is no corresponding structural eigenfrequency.

Coupling Among Fundamental Fluid Waves

In the following, the coupling among the fundamental fluid waves with ND 12,14 and 16 with incommensurable frequencies is investigated. Therefore, the fundamental waves (and their higher harmonics) are isolated from each other. At first, for each fundamental frequency $\omega_{\mathrm{ND}n}$, $n = 12,14,16$, a subset $\hat{\boldsymbol{u}}^{\mathrm{s}}_k|_{\mathrm{ND}n}$, $k = 1,2,3$ of the Fourier coefficients $\hat{\boldsymbol{u}}^{\mathrm{s}}_{l,m}$, $(l,m) \in \mathscr{K}$ is extracted from the modal displacements $\boldsymbol{u}^{\mathrm{s}}$ of the LTO solution via a Discrete Fourier Transformation (DFT). Each subset conforms to a harmonic set of the fundamental wave with a single fundamental frequency and its higher harmonics, in other words, it conforms to a periodic motion / LCO. For example, the Fourier coefficients $\hat{\boldsymbol{u}}^{\mathrm{s}}_k|_{\mathrm{ND}14}$, $k = 1,2,3$ correspond to $\hat{\boldsymbol{u}}^{\mathrm{s}}_{l,m}$, $(l,m) \in \{(0,1),(0,2),(0,3)\}$ and the resulting harmonic set has a fundamental frequency $\omega_{\mathrm{ND}14}$ and a fundamental ND of 14. The sampling window for the DFTs is adjusted for each fundamental frequency in order to achieve the best result and to reduce spectral leakage. Subsequently, for each fundamental frequency $\omega_{\mathrm{ND}n}$ a periodic blade motion

$$\boldsymbol{u}^{\mathrm{s}}(t)|^{\mathrm{HB}}_{\mathrm{ND}n} \approx \Re\left\{\sum_{k=1}^{H^{\mathrm{s}}} e^{ik\omega_{\mathrm{ND}n}t}\,\hat{\boldsymbol{u}}^{\mathrm{s}}_k|_{\mathrm{ND}n}\right\}. \tag{9}$$

with $H^{\mathrm{s}} = 3$ is prescribed. Since a single fundamental frequency $\omega_{\mathrm{ND}n}$ is present for each subset of Fourier coefficients $\hat{\boldsymbol{u}}^{\mathrm{s}}_k|_{\mathrm{ND}n}$, the HB method is very suitable to determine the resulting harmonic modal aerodynamic forces $\hat{\boldsymbol{f}}^{\mathrm{a}}_k|^{\mathrm{HB}}_{\mathrm{ND}n}$ with a harmonic truncation order of $H^{\mathrm{a}} = 4$ (harmonic convergence for $H^{\mathrm{s}} = 5$ and $H^{\mathrm{a}} = 6$ could be confirmed). Due to the harmonic set approach, the HB method only approximates the aerodynamic forces $\hat{\boldsymbol{f}}^{\mathrm{a}}_k|^{\mathrm{HB}}_{\mathrm{ND}n}$ since

a.) the coupling among the sets is neglected and
b.) several Fourier modes (linear combinations of the two fundamental frequencies) which participate in the LTO are not contained in any harmonic set at all.

The harmonic modal aerodynamic forces obtained with the HB method $\hat{\boldsymbol{f}}^{\mathrm{a}}_k|^{\mathrm{HB}}_{\mathrm{ND}n}$ are compared to the ones directly computed from the coupled LTO solution $\hat{\boldsymbol{f}}^{\mathrm{a}}_k|^{\mathrm{LTO}}_{\mathrm{ND}n}$ (again using a DFT with a carefully chosen window). In Fig. 8a $\hat{\boldsymbol{f}}^{\mathrm{a}}_k|^{\mathrm{HB}}_{\mathrm{ND}14}$ and $\hat{\boldsymbol{f}}^{\mathrm{a}}_k|^{\mathrm{LTO}}_{\mathrm{ND}14}$ for three harmonics of the fundamental ND of 14 are shown. The colors identify the indices of the modes associated to the ND (10 mode families per ND are used for the ROM). For the first harmonic they agree perfectly while for an increasing harmonic index the deviations get larger. In case of the second harmonic some similarity can still be observed, but for the third harmonic there is no agreement at all (except the order of magnitude of the forces). In Fig. 8b the same is depicted for the fundamental wave of ND 10. While good agreement for the first harmonic can be observed, the second and third harmonic do not show any similarity of the results. For other harmonic sets with the fundamental NDs 12, 16 and 18 the results are similar. Essentially, the observation can be made, that the first harmonic forces for all harmonic sets agree quite well with the LTO result. For higher harmonics (especially when the vibrational amplitude of the fundamental harmonic is relatively low) deviations with respect to the LTO result occur. Here, the coupling among harmonic sets of the LTO solution on the fluid side is visible.

SUMMARY AND CONCLUSIONS

An LTO of a shrouded LPT with a sophisticated numerical model is presented and the harmonic content of it is investigated. The observed pattern of the participating harmonics motivated the formulation of an alternative basis of the Fourier space for the description of quasi-periodic blade vibrations. This alternative basis leads to a very compact grid for the relevant harmonic indices. This observation could be very helpful for the prospective analysis of LTOs with frequency domain methods, where a set of harmonics must be chosen before a simulation is carried out. While it is known that the coupling of the participating fundamental waves on the structural side is of great importance due to the strongly nonlinear contact forces, in this study the coupling among waves on the fluid side is numerically investigated. It is empirically shown, that the aerodynamic forces can to some extend be approximated with the HB method using the harmonic set approach, where coupling among harmonic sets is neglected. This observation should be considered to be part of an intermediate research result and motivates the development of novel coupled frequency domain methods suitable for the simulation of LTOs with multiple fundamental frequencies. One concept includes the application of a Multidimensional Harmonic Balance (MHB) Method [24] to the fluid and the structure which would be an extension of the FD-FSI solver developed in [7, 8]. The presented study indicates, that the application of the (computationally more expensive) MHB method on the fluid side might not be necessary and the HB approach could turn out to be sufficient. It remains to be evaluated, if the error of the harmonic set approach, which is especially observable for higher harmonics, is acceptable for the development of coupled frequency domain FSI solvers which are capable of simulating LTOs.

ACKNOWLEDGMENT

The research project was financially supported by the German Research Foundation (DFG) (funding no. 382141955) and the FVV (Research Association for Combustion Engines eV) (FVV funding no. 6013081). The research project was performed by the Institute of Propulsion Technology (IAT) at the

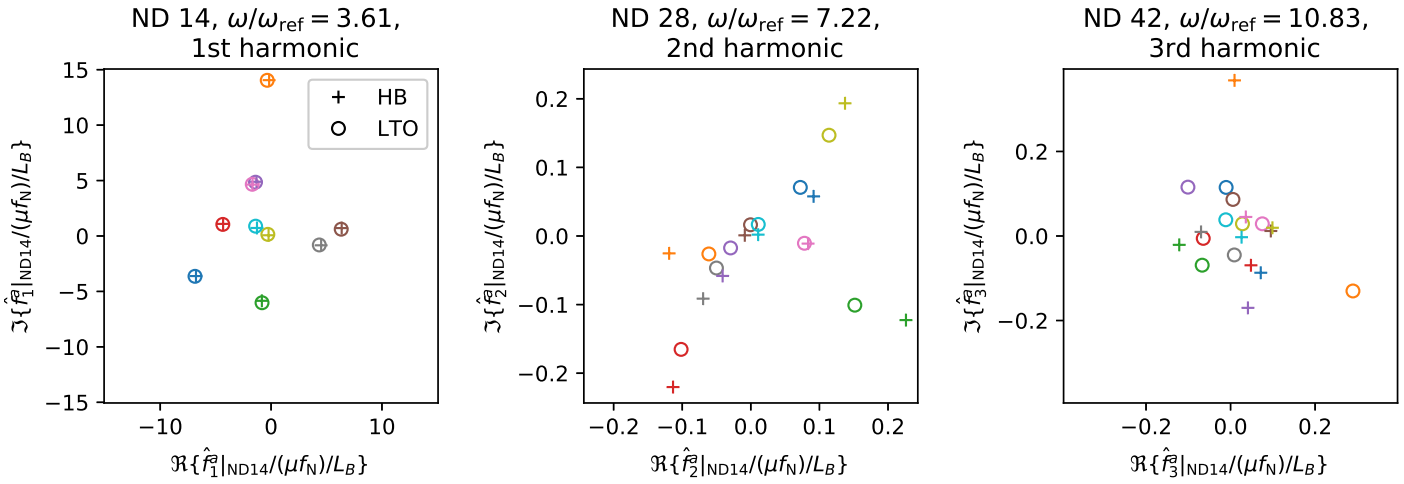

(a) Harmonic set with fundamental ND 14.

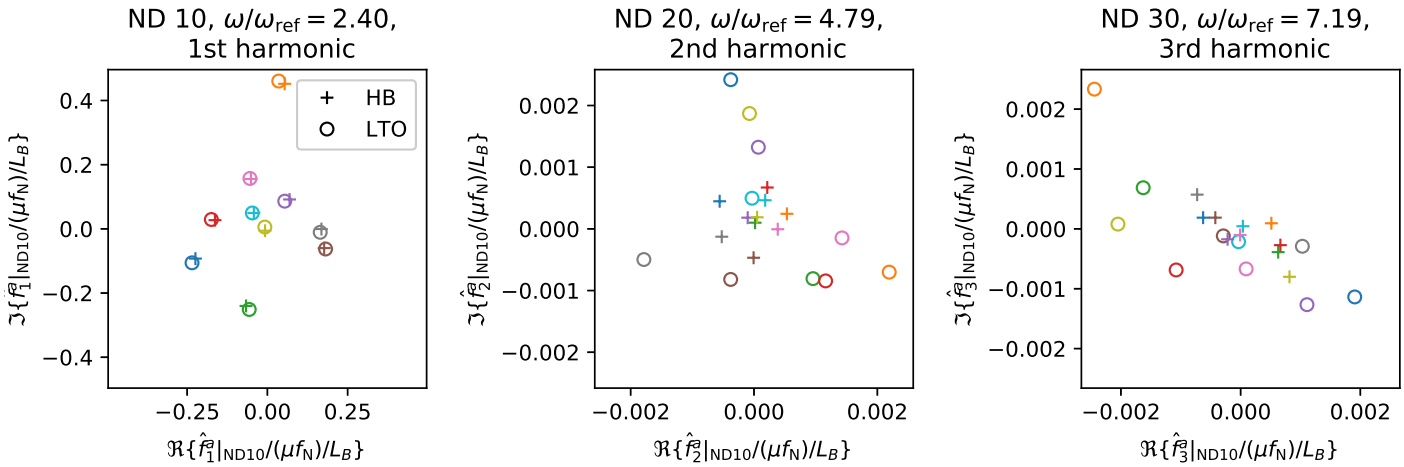

(b) Harmonic set with fundamental ND 10.

FIGURE 8: Modal aerodynamic forces (real and imaginary part) on complex plane: LTO vs. HB

German Aerospace Center under the direction of Prof. Reinhard Mönig and by the Institute of Aircraft Propulsion Systems (ILA) at University of Stuttgart under the direction of Jun.-Prof. Malte Krack. The project was conducted by an expert group under the direction of Dr. Andreas Hartung (MTU Aero Engines AG). The authors greatfully acknowledge the support received from the FVV (Research Association for Combustion Engines eV) and the DFG (German Research Foundation).

REFERENCES

[1] Waite, J. J., and Kielb, R. E., 2016. "The impact of blade loading and unsteady pressure bifurcations on low-pressure turbine flutter boundaries". *Journal of Turbomachinery,* ***138***(4).

[2] Waite, J. J., and Kielb, R. E., 2016. "Shock structure, mode shape, and geometric considerations for low-pressure turbine flutter suppression". In Turbo Expo: Power for Land, Sea, and Air, Vol. 49842, American Society of Mechanical Engineers, p. V07BT34A009.

[3] Firrone, C. M., and Zucca, S., 2011. "Modelling friction contacts in structural dynamics and its application to turbine bladed disks". *Numerical Analysis-Theory and Application,* ***14***, pp. 301–334.

[4] Lassalle, M., and Firrone, C., 2018. "A parametric study of limit cycle oscillation of a bladed disk caused by flutter and friction at the blade root joints". *Journal of Fluids*

and Structures, ***76***, pp. 349–366.

[5] Martel, C., Corral, R., and Ivaturi, R., 2014. "Flutter amplitude saturation by nonlinear friction forces: Reduced model verification". *Journal of Turbomachinery,* ***137***(4), p. 041004.

[6] Berthold, C., Frey, C., Dhondt, G., and Schönenborn, H., 2018. "Fully coupled aeroelastic simulations of limit cycle oscillations in the time domain". In Proceedings of the 15th ISUAAAT.

[7] Berthold, C., Gross, J., Frey, C., and Krack, M., 2020. "Analysis of friction-saturated flutter vibrations with a fully coupled frequency domain method". *Journal of Engineering for Gas Turbines and Power,* ***142***(11), p. 111007.

[8] Berthold, C., Gross, J., Frey, C., and Krack, M., 2021. "Development of a fully-coupled harmonic balance method and a refined energy method for the computation of flutter-induced limit cycle oscillations of bladed disks with nonlinear friction contacts". *Journal of Fluids and Structures,* ***102***, p. 103233.

[9] Krack, M., 2015. "Nonlinear modal analysis of nonconservative systems: Extension of the periodic motion concept". *Computers and Structures,* ***154***, pp. 59–71.

[10] González-Monge, J., Rodríguez-Blanco, S., and Martel, C., 2021. "Friction-induced traveling wave coupling in tuned bladed-disks". *Nonlinear Dynamics*, pp. 1–11.

[11] Woiwode, L., Gross, J., and Krack, M., 2021. "Effect of modal interactions on friction-damped self-excited vibrations". *Journal of Vibration and Acoustics,* ***143***(3), p. 031003.

[12] Krack, M., Panning-von Scheidt, L., and Wallaschek, J., 2016. On the interaction of multiple traveling wave modes in the flutter vibrations of friction-damped tuned bladed disks. Proceedings of the ASME Turbo Expo, Seoul, South Korea, GT2016-56126, pp. 1-11.

[13] Gross, J., and Krack, M., 2020. "Multi-wave vibration caused by flutter instability and nonlinear tip-shroud friction". *Journal of Engineering for Gas Turbines and Power,* ***142***(2).

[14] Krack, M., Salles, L., and Thouverez, F., 2017. "Vibration prediction of bladed disks coupled by friction joints". *Archives of Computational Methods in Engineering,* ***24***(3), pp. 589–636.

[15] Woiwode, L., Vakakis, A. F., and Krack, M., 2021. "Analysis of the non-periodic oscillations of a self-excited friction-damped system with closely spaced modes". *Nonlinear Dynamics,* ***106***(3), Nov., pp. 1659–1673.

[16] Berthold, C., Gross, J., Frey, C., and Krack, M., 2022. "Fully Coupled Analysis of Flutter Induced Limit Cycles: Frequency vs. Time Domain Methods". Vol. Structures and Dynamics of *Turbo Expo: Power for Land, Sea, and Air - submitted and accepted*.

[17] Craig, R. R., and Bampton, M. C., 1968. "Coupling of substructures for dynamic analyses". *AIAA Journal,* ***6***(7), pp. 1313–1319.

[18] Wilcox, D. C., 1988. "Reassessment of the scale-determining equation for advanced turbulence models". *AIAA J.,* ***26***(11), November, pp. 1299–1310.

[19] Kersken, H.-P., Ashcroft, G., Frey, C., Wolfrum, N., and Korte, D., 2014. "Nonreflecting boundary conditions for aeroelastic analysis in time and frequency domain 3D RANS solvers". In Proceedings of ASME Turbo Expo 2014.

[20] Srinivasan, A., 1997. "Flutter and resonant vibration characteristics of engine blades". *Journal of Engineering for Gas Turbines and Power,* ***119***, Oct., pp. –.

[21] Berthold, C., Frey, C., and Schönenborn, H., 2018. *Coupled Fluid Structure Simulation Method in the Frequency Domain for Turbomachinery Applications*.

[22] Newmark, N. M., 1959. "A method of computation for structural dynamics". *Journal of the engineering mechanics division,* ***85***(3), pp. 67–94.

[23] Ashcroft, G., Frey, C., and Kersken, H.-P., 2014. "On the development of a harmonic balance method for aeroelastic analysis". In 6th European Conference on Computational Fluid Dynamics (ECFD VI).

[24] Guskov, M., and Thouverez, F., 2012. "Harmonic balance-based approach for quasi-periodic motions and stability analysis". *Journal of Vibration and Acoustics,* ***134***(3), pp. 031003/1–031003/11.